EPJ manuscript No.
(will be inserted by the editor)

Unusual persistence of superconductivity against high magnetic fields in the strongly-correlated iron-chalcogenide film FeTe:O$_x$

I. K. Dimitrov[1a], W. D. Si[1], W. Ku[1], S. J. Han[1], and J. Jaroszynski[2]

[1] Condensed Matter Physics and Materials Science Department, Brookhaven National Laboratory, Upton, New York 11973-5000, USA
[2] National High Magnetic Field Laboratory, Florida State University, Tallahassee, Florida 32310, USA

Received: date / Revised version: date

Abstract. We report an unusual persistence of superconductivity against high magnetic fields in the iron chalcogenide film FeTe:O$_x$ below 2.52 K. Instead of saturating like a mean-field behavior with a single order parameter, the measured low-temperature upper criticial field increases progressively, suggesting a large supply of superconducting states accessible via magnetic field or low-energy thermal fluctuations. We demonstrate that superconducting states of finite momenta can be realized within the conventional theory, despite its questionable applicability. Our findings reveal a fundamental characteristic of superconductivity and electronic structure in the strongly-correlated iron-based superconductors.

PACS. 74.70.Xa Chalcogenides: noncuprate superconductors – 74.20.Mn Nonconventional mechanisms in superconductivity – 74.25.Dw Superconductivity phase diagrams

1 Introduction

Ever since the discovery of iron-based superconductors in 2008 [1], an avalanche of research effort was aimed at understanding the pairing mechanisms behind the origins of superconductivity in these materials [2]. These novel systems have shown similarities and differences to both high T_c and heavy fermion systems [2]. What has made the study of iron-based materials even more elusive is that some experimental data suggest that the antiferromagnetic and superconducting order parameters compete in certain systems, while they coexist in others [3,4,5,6,7]. In very recent times it has been suggested that magnetic and structural instabilities can potentially form the superconducting state [2].

However, in order to understand the nature of the superconducting state and its underlying mechanism, it is imperative to gain insight into a materials electronic structure [8,9]. One of the most relevant approaches to studying the electronic structure of superconductors has come in the way of exploring their magnetic responses to an external magnetic field, H, as a function of temperature, T. In the case of BCS superconductors, the upper critical field, H_{c2}, has been used as a measure of electronic coherence [8], as well as an indicator of the relevant pairbreaking mechanisms [8,10,11]. Detailed analyses of the $H-T$ phase diagrams of iron pnictides and chalcogenides have been utilized to suggest that they are multi-band superconductors with unconventional pairing mechanisms [12, 13].

Here, we report a striking persistence of superconductivity against high magnetic fields in the iron chalcogenide film FeTe:O$_x$ below 2.52 K. The measured low-temperature H_{c2} increases progressively, showing a striking inflection, instead of the saturation expected from a mean-field theory with a single order parameter. This suggests the presence of a large supply of superconducting states accessible via magnetic field. Additionally, our observations suggest that the rapid reduction of the upper critical field with increasing temperature (concomitantly with the superfluid density) is a consequence of thermal fluctuations involving these states. We explore a scenario of Cooper pairs with finite center-of-mass momentum and find that, while not perfectly justifiable, it is consistent with our data below $T \approx 2.52$ K. Our findings reveal a fundamental characteristic of superconductivity and electronic structure in the strongly-correlated iron-based superconductors.

The procedure for the FeTe:O$_x$ film deposition was described in detail elsewhere [14]. A zero-field temperature scan of the resistivity of our sample exhibits a T_c of 7.05 K. Currently, the mechanism of oxygen-induced superconductivity in FeTe:O$_x$ films is still unknown [14,15]. Further investigations to sort out the effects of oxygen in this class of films present an important scientific objective for the field. Here, however, we focus exclusively on the behavior of superconductivity due to the presence of an external magnetic field.

The paper is organized as follows. In Sec. 2, we acquaint the reader with the experimental setup and the

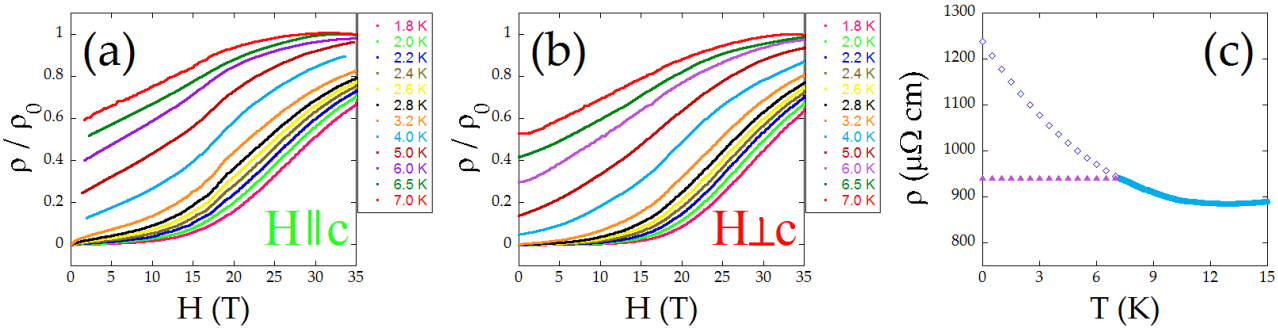

Fig. 1. Magnetic field dependence of the normalized resistivity of FeTe:O_x at select temperatures with (a) $H \parallel c$ and (b) $H \perp c$. ρ_0 denotes the sample resistance of the normal state at $H = 35$ T, while ρ is the measured resistance. ρ_0 is defined according to the temperature scan from 15 K to 7 K at 35 T, shown in light blue in (c). The definition for $\rho_0(T)$ for the data analysis below 7 K is obtained from a third-order polynomial fit through the 7 – 15 K data (shown in dark-blue empty rhombi in (c)). The data is also analyzed using an alternative definition for ρ_0, which assumes a constant ρ_0 below 7 K (depicted in the straight line of filled purple triangles in (c)) [16].

details of the data analysis of the resistivity data, from which we extract the superconducting $H - T$ phase diagram of our FeTe:O_x thin film sample in both $H \parallel ab$ and $H \parallel c$ configurations. In Sec. 3, we present the calculation of the center-of-mass momentum, Q, from the resultant phase diagram, taking into account the mass anisotropy, which we directly measure in our experiment, and various other parameters. Here, we also provide a discussion of a possible interpretation of our combined experimental and theoretical results. Finally, in Sec. 4, we close our treatise with a brief summary of our findings and claims.

2 Experimental Techniques and Data Analysis Details

ac transport measurements of the parallel and perpendicular components of H_{c2} with respect to the crystallographic c axis, $H_{c2}^{\parallel c}(T)$ and $H_{c2}^{\perp c}(T)$, were carried out at the National High Magnetic Field Laboratory in Tallahassee, Florida in dc magnetic fields from 0 to 35 T. The field was applied at a rate of 5 T/min during increasing field ramps at fixed temperatures. The resistivity, $\rho(T)$, was measured via phase-sensitive lock-in detection ($I = 5$ μA; $f = 17$ Hz) at a variety of T's from 1.5 – 8 K. The data from the field scans were normalized with respect to the normal state resistivity, $\rho_0(T)$, obtained from temperature scans at $H = 35$ T, from 15 K to 7 K. The normalized resistivities for $H \parallel c$ and $H \perp c$ at select temperatures are shown in Fig. 1(a) and (b), respectively [16].

The mid-point of the normalized resistivity, (50% of $\rho(T)/\rho_0(T)$), was chosen to define the experimental $H_{c2}(T)$ [17]. $H \perp c$ and $H \parallel c$ are shown in Fig. 2. We point to a very steep increase in the H_{c2} curves near T_c ($-dH_{c2}^{\perp c}/dT|_{H\leq 10T} \approx 9.24$ T/K and $-dH_{c2}^{\parallel c}/dT|_{H\leq 10T} \approx 6.06$ T/K). It is also to be noted that $\rho(T, 35\text{T})$ in our sample exhibits an insulator-like behavior right above the superconducting transition (see Fig. 1(c)), despite the fact that it has a Fermi surface and is expected to behave like a metal.

3 Experimental Techniques and Data Analysis Details

The most remarkable observation here is the unusual persistence of superconductivity against high magnetic fields at low temperatures, manifest in an inflection of the phase boundary of the $H - T$ phase diagram (Fig. 2), which is clearly present in the $H \perp c$ case, and less drastically in the $H \parallel c$ one. Apparently, at low temperatures ($T < 2.5$ K), the superconductivity survives much stronger fields by readjusting itself in some non-trivial way. This is in great contrast to the phase diagram saturation characteristic of a BCS superconductor described by a mean-field theory of a single order parameter. Generally speaking (without involving any specific theory), this indicates that there is a large number of low-energy superconducting states of different momenta (in a flat energy landscape) accessible via magnetic field. The thermal fluctuations involving these states cause the rapid reduction of H_{c2} (and the superfluid density) as the temperature increases. Given the large gap size of the system ($\Delta \sim 3.5 k_B T_c$) [18,19], such fluctuations are likely in the phase (not amplitude) of the order parameter. This strong coupling behavior is expected in the underdoped samples [20] (like the present one) with correlated electronic structure [21,22], as evident from the proximity to magnetic/orbital/structural orders.

Nonetheless, due to the poor understanding of such a strong coupling regime, we stay within the conventional framework of BCS theory, as this is the only currently-available approach. The Werthamer-Helfand-Hohenberg (WHH) theory was developed to describe the orbital-limited upper critical field, $H_{c2}^O(T)$, for a single active band in the weakly-coupled limit: $H_{c2}^O(0) = -0.69 dH/dT|_{T=T_c} T_c$ [10]. Applying it to our FeTe:O_x thin film $H - T$ phase diagram yields $H_{c2}^O(0) = 44.95$ T and 29.48 T in $H \perp c$ and $H \parallel c$, respectively. On the other hand, the expected paramagnetic pair-breaking (Pauli-limited) upper critical field, $H_{c2}^P(0)$, in the same sample is estimated to be 1.86 $T_c = 13.11$ T from the Clogston-Chandrasekhar (CC) theory [11]. In a related transport measurement, Khim *et al.*

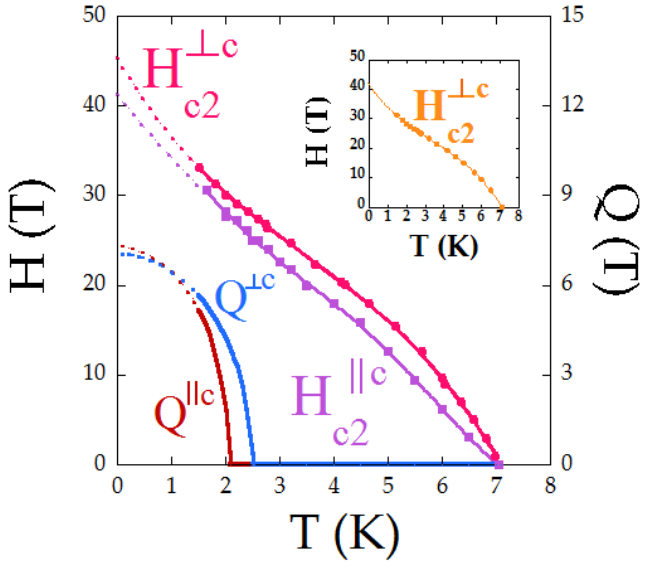

Fig. 2. Phase diagram constructed from the normalized resistance versus temperature data. The $H_{c2}(T)$ for $H \perp c$ (pink solid circles) and $H \parallel c$ (violet solid squares) were defined at 50% of $\rho_0(T)$ from the field scans (Fig.1(a) and (b)). The dotted lines below $T = 1.5$ K are guides for the eye. The calculated values of $Q^{\perp c}(T)$ and $Q^{\parallel c}(T)$ are shown in red and blue, respectively. Inset: Shown is the $H-T$ phase diagram for $H \perp c$ obtained by the alternative analysis condition, setting ρ_0 to be a constant below 7 K.

argued that the much larger H_{c2}^O's in comparison to the H_{c2}^P measured in a $FeTe_{0.6}Se_{0.4}$ single crystal suggests that these observations could imply the importance of paramagnetic pair-breaking effects, or be due to multi-band scattering in the latter system [12]. Notwithstanding the above interpretation, both WHH and CC are derived in the weakly-coupled limit, while their validity in a strongly coupled, non-BCS system such as Fe(Te,Se) remains dubious [23,24,12].

Within BSC, the finite momentum superconductivity is explained within the FFLO picture [25,26]. This should be considered as one possible scenario consistent with the above general considerations, but not necessarily representing the only (or even the correct) microscopic picture. The FFLO state is marked by a smaller condensation energy, but also by a lower Zeeman energy, compared to the normal state, resulting in an overall suppression of the normal state at magnetic fields higher than $H_{c2}^P = 2\Delta/g\mu_B$ (Clogston limit [11]), where Δ, g and μ_B stand for the superconducting gap, the gyromagnetic ratio of a free electron, and the Bohr magneton, respectively [25,26,27]. The FFLO state has been reported in a number of organic [27,28], and heavy fermion superconductors [27,29]. In general, strong type II superconductors with large Maki parameters, $\alpha_M = \sqrt{2}H_{c2}^O/H_{c2}^P$, in the clean limit, $\xi \ll l$, are the typical candidates for FFLO state systems, where ξ and l denote the superconducting coherence length and the electronic mean free path, respectively [27].

Subsequently, we set out to analyze the H–T phase diagram of $FeTe:O_x$ using the established FFLO theoretical framework [30]. We minimized the equation of state for the parameter $q\,(T)\,|_{H=H_{c2}}$ of a two-band model which accomodates orbital and paramagnetic pair-breaking mechanisms (Equation (1)) at each point in the H versus T phase diagram [30]. Finally, we used this parameter to derive $Q(T)|_{H=H_{c2}}$ [30]:

$$a_1(ln\,t+U_1)+a_2(ln\,t+U_2)+(ln\,t+U_1)(ln\,t+U_2)=0 \quad (1)$$

where $a_1 = (\lambda_0 + \lambda_-)/2w$, $a_2 = (\lambda_0 - \lambda_-)/2w$, with $\lambda_- = \lambda_{11} - \lambda_{22}$, $\lambda_0 = (\lambda_-^2 + 4\lambda_{12}\lambda_{21})^{1/2}$, and $w = \lambda_{11}\lambda_{22} - \lambda_{12}\lambda_{21}$. λ_{ij} $(i,\ j = 1,\ 2)$ define the coupling constants used in the theory [30]. In the limit of strong interband pairing ($\lambda_{12}\lambda_{21} \gg \lambda_{11}\lambda_{22}$), we obtain $\lambda_{11} = \lambda_{22} = 0$ and $\lambda_{12} = \lambda_{21} = 0.5$, leading to $a_1 = a_2 = -1$ [30]. In the above equation we used the integral form for U_1 [30]:

$$U_1 = \ln(4\gamma) + \frac{te^{q^2}}{\sqrt{b}}\int_q^\infty du e^{-u^{-2}},$$
$$\Im\left\{\ln\frac{\Gamma\left[1/2+i\left(\alpha b+u\sqrt{b}\right)/t\right]}{\Gamma\left[1/2+i\left(\alpha b-u\sqrt{b}\right)/t\right]}\right\} \quad (2)$$

where $\gamma \approx 1.78$ and $t = T/T_c$. The rest of the quantities are defined as follows:

$$q = \left(\frac{Q_z^2\phi_0\epsilon_1}{2\pi H}\right)^{1/2},\ b = \frac{\hbar^2 v_1^2 H}{8\pi\phi_0 k_B^2 T_c^2 \omega_1^2},\ \alpha = \frac{4\mu\phi_0 k_B T_c \omega_1}{\hbar^2 v_1^2} \quad (3)$$

where Q_z, ϕ_0 and μ stand for the projection of vector Q along the field direction, flux quantum and the magnetic moment of a quasiparticle, respectively, while ϵ_1, v_1, ω_1 represent the mass anisotropy, Fermi velocity and the Eliashberg constant, $\omega_1 = 1 + \lambda_{11} + |\lambda_{12}|$, for band *1*. U_2 is obtained by replacing ω_1 with $\omega_2 = 1 + \lambda_{22} + |\lambda_{21}|$, b with $b\eta$ (except terms $\propto \alpha b$), and q with $q\sqrt{s}$ in U_1. Here, $\eta = v_2^2/v_1^2$, $s = \epsilon_2/\epsilon_1$, and v_2 and ϵ_2 represent the Fermi velocity and mass anisotropy for band *2*, respectively [30,13]. The Fermi velocity used in the calculation, $v_1 = 0.7$ eV·Å$= 1.0635 \times 10^5$ m/s, was obtained from an ARPES measurement on a $Fe_{1+x}Te$ single crystal [31]. $\mu = 2.2\mu_0$ [22], where μ_0 is the Bohr magneton, in order to calculate $b\,(T,H)$ and α. ϵ_1 is related to the anisotropy parameter, γ_H, by $\epsilon_1 = 1/\sqrt{\gamma_H}$, and $\gamma_H(T)$ was derived from $\gamma_H(T) = H_{c2}^{\perp c}(T)/H_{c2}^{\parallel c}(T)$ (see Fig. 3) and taken to be equal to 1 for convenience. The field and mass anisotropies, γ_H and γ_m, cannot be necessarily considered equal as in the case of the anisotropic single-band superconductors [32,33] and the discrepancy between the two has been interpreted to be a signature of multi-band physics in a $LaFeAsO_{1-x}F_x$ oxypnictide film [33]. Furthermore, we performed an angular-dependent transport measurement of $H_{c2}(T = 1.75)$ K (see Fig. 3). $H_{c2}(\phi, 1.75\,K)$ is rather nicely fitted with a calculation based on the single band anisotropic Ginzburg-Landau theory (Inset of Fig. 3) [34]. Finally, we approximated the ratio of the mass anisotropies in the two bands as $s = 1$ while $\eta =$

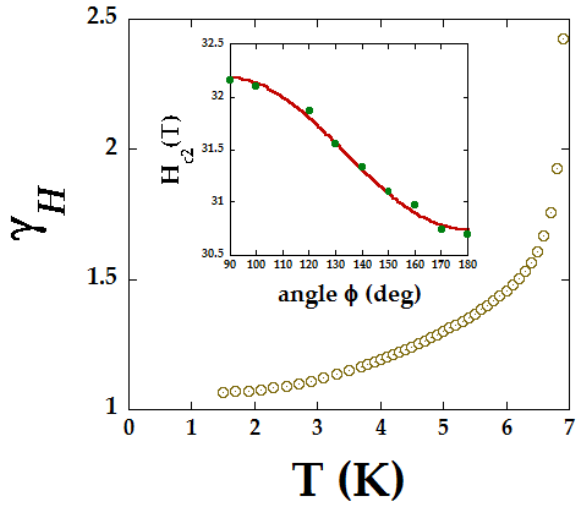

Fig. 3. The anisotropy parameter, $\gamma_H = H_{c2}^{\perp c}/H_{c2}^{\parallel c}$, as a function of temperature, obtained from $H_{c2}^{\perp c}$ and $H_{c2}^{\parallel c}$, shown in Fig. 2. Inset: shown is the angular dependence of $H_{c2}(T)$ at $T = 1.75$ K from $\phi = 90°$ ($H \perp c$) to $\phi = 180°$ ($H \parallel c$) (in filled green circles), obtained from 35 – 0 T field scans ($\mathrm{d}H/\mathrm{d}T = -7$ T/min). The solid red line is a fit of $H_{c2}(\phi) = H_{c2}^{\perp c}\cdot[\cos^2(\phi) + \sin^2(\phi)/{\gamma_m}^2(T)]^{-0.5}$ through the data points, yielding $H_{c2}^{\perp c}(1.75\,K) = 30.75$ T and $\gamma_m(1.75\,K) = 1.05$.

0.3 [13]. α was calculated to be $0.016(\Delta^w/k_B)$, where Δ^w is the superconducting gap in the weakly-coupled limit ($\Delta^w \approx 1.74 k_B T_c$). However, a typical gap observed in FeTe superconductors is on the order of $3.5 k_B T_c$ [18,19]. Thus, in order to get the correct value for α we used $\Delta = 3.5 k_B T_c$ instead, finally obtaining $\alpha = 0.4$. No further rescaling of the parameters q, α and b was pursued.

The results of our calculation for $Q^{\perp c}(T)|_{H=H_{c2}}$ and $Q^{\parallel c}(T)|_{H=H_{c2}}$ are shown in units of $1/\sqrt{\phi_0}$ in Fig. 2. Remarkably, we obtain $H_{c2}^{\perp c}(0) \approx 42$ T and $H_{c2}^{\parallel c}(0) \approx 44$ T upon calculating the $H_{c2}(0)$ in the paramagnetic limit, $Q(0) \approx 2\mu H/\hbar v_F$ [27]. $H_{c2}^{\perp c}(0)$ obtained from $Q^{\perp c}(\mathrm{T})|_{H=H_{c2}}$ agrees nicely with the guide for the eye drawn in Fig. 2 for $H_{c2}^{\perp c}(0)$, while the respective result for $H_{c2}^{\parallel c}(0)$ suggests that the $H_{c2}^{\parallel c}(\mathrm{T})$ curve is slightly steeper than the guide for the eye. It is to be noted that $Q^{\perp c}(\mathrm{T})|_{H=H_{c2}}$ starts to exhibit non-zero values at 2.52 K, just above the unusual upturn in $H_{c2}^{\perp c}(T)$, which translates to $0.36\,T_c$.

We note, however, that the measured $\gamma_H(T)$ is very close to unity, especially in the temperature range where the calculated $Q(T)$ acquires non-zero values (see Fig. 3). The lower anisotropy is not favorable for the formation of an FFLO state [30], and especially surprising is the fact that we measure non-zero $Q(T)$ which coincides with a very unusual behavior in $H_{c2}(T)$ in a system which is not in the clean limit. Also, the weakly-coupled two band scenario entertained by Kidszun *et al.* [33] would be inconsistent with the strong intraband scattering and Pauli-limited H_{c2}'s present in iron-based superconductors [30].

All of these suggest that while the general physical considerations concerning the large supply of superconducting states is reasonable, the detailed microscopic understanding remains elusive, and likely to be enriched by the strongly-correlated nature of the electronic structure of this system. The observed unusual persistence of superconductivity against high magnetic fields not only reveals a fundamental characteristic of the superconductivity in this system, but also puts a strong constraint on the microscopic understanding of the electronic structure of this new class of superconductors.

4 Summary

In conclusion, we have found a striking persistence of superconductivity in a FeTe:O_x thin film at high magnetic fields, especially when the field is applied perpendicular to the crystallographic c plane. The upturn in the slope of the superconducting H-T phase boundary suggests the presence of a large supply of superconducting states accessible via magnetic field. We stipulate that our observations suggest that the rapid reduction of the upper critical field with increasing temperature (concomitantly with the superfluid density) is a consequence of thermal fluctuations involving these states.

In order to gain a deeper understanding into the nature of the superconducting state, we explored a scenario of Cooper pairs in the weakly-coupled limit with finite center-of-mass momentum. By utilizing a theoretical approach developed by A. Gurevich [30], we find that even if the above model is not fully justifiable, it is still consistent with our data, since we observe the emergence of a non-zero Q at $T \leq 2.5$ K.

We thus conclude that this observed exotic behavior in the superconducting phase diagram of FeTe:O_x might be a consequence of the strongly-correlated nature of this particular system.

5 Acknowledgements

The work at Brookhaven National Laboratory was supported by the Office of Science, U.S. Department of Energy, Materials Sciences and Engineering Division, under Contract No. DE-AC02-98CH10886. A portion of this work was performed at the National High Magnetic Field Laboratory, which is supported by NSF Cooperative Agreement No. DMR-0654118 by the State of Florida, and by the DOE. I.K.D. wishes to thank Vyacheslav Solovyov and Silvia Haindl for fruitful discussions.

References

1. Yoichi Kamihara, Takumi Watanabe, Masahiro Hirano, and Hideo Hosono, J. Am. Chem. Soc. **130**, 3296 (2008).
2. I. I. Mazin, Nature **464**, 183 (2010).
3. Jun Zhao, Q. Huang, Clarina De La Cruz, Shiliang Li, J. W. Lynn, Y. Chen, M. A. Green, G. F. Chen, G. Li, Z. Li, J. L. Luo, N. L. Wang, and Pengcheng Dai, Nature Mater. **7**, 953 (2008).

4. C. Lester, Jiun-Haw Chu, J. G. Analytis, S. C. Capelli, A. S. Erickson, C. L. Condron, M. F. Toney, I. R. Fisher, and S. M. Hayden, Phys. Rev. B **79**, 144523 (2009).
5. S. Nandi, M. G. Kim, A. Kreyssig, R. M. Fernandes, D. K. Pratt, A. Thaler, N. Ni, S. L. Bud´ko, P. C. Canfield, J. Schmalian, R. J. McQueeney, and A. I. Goldman, Phys. Rev. Lett. **104**, 057006 (2010).
6. L. Chauvière, Y. Gallais, M. Cazayous, M. A. Measson, A. Sacuto, D. Colson and A. Forget, Phys. Rev. B **82**, 180521(R) (2010).
7. F. Hardy, P. Burger, T. Wolf, R. A. Fisher, P. Schweiss, P. Adelmann, R. Heid, R. Fromknecht, R. Eder, D. Ernst, H. v. Löhneysen and C. Meingast, Eur. Phys. Lett. **91**, 47008 (2010).
8. M. Tinkham, *Introduction to Superconductivity* (Second Edition, Dover Publications, Inc., Mineola, New York, 1996).
9. P. G. De Gennes, *Superconductivity of Metals and Alloys* (Westview Press, 1999).
10. N. R. Werthamer, E. Helfand and P. C. Hohenberg, Phys. Rev. **147**, 295 (1966).
11. A. M. Clogston, Phys. Rev. Lett. **9**, 266 (1962); B. S. Chandrasekhar, Appl. Phys. Lett. **1**, 7 (1962).
12. Seunghyun Khim, Jae Wook Kim, Eun Sang Choi, Yunkyu Bang, Minoru Nohara, Hidenori Takagi, and Kee Hoon Kim, Phys. Rev. B **81**, 184511 (2010).
13. K. Cho, H. Kim, M. A. Tanatar, Y. J. Song, Y. S. Kwon, W. A. Coniglio, C. C. Agosta, A. Gurevich, and R. Prozorov, Phys. Rev. B **83**, 060502(R) (2011).
14. Weidong Si, Qing Jie, Lijun Wu, Juan Zhou, Genda Gu, P. D. Johnson, and Qiang Li, Phys. Rev. B **81**, 092506 (2010).
15. Qiang Li, Weidong Si and Ivo K. Dimitrov, Rep. Prog. Phys. **74**, 124510 (2011) and references therein.
16. In order to avoid certain artifacts which may potentially arise in the data analysis from overestimation of $\rho_0(T)$ from the polynomial fit, we obtained the superconducting phase diagram of FeTe:O_x also utilizing a much more rigorous criterion, which assumes that $\rho_0(T)$ remains constant below 7 K (Fig. 1(c)). The resultant $H_{c2}^{\perp c}(T)$ curve is shown in the Inset of Fig. 2 and we note that despite the fact that it is down-shifted with respect to the $H_{c2}^{\perp c}(T)$ obtained using the standard scheme, both phase diagrams show the same signature behavior.
17. The normal state below $T \approx 5$ K could not be reached fully due to the very high $H_{c2}(T)$ of the sample. The low-field data ($H \sim 0 - 9$ T) were confirmed by means of temperature scans performed in a Physical Property Measurement System by Quantum Design.
18. K. Nakayama, T. Sato, P. Richard, T. Kawahara, Y. Sekiba, T. Qian, G. F. Chen, J. L. Luo, N. L. Wang, H. Ding, and T. Takahashi, Phys. Rev. Lett. **105**, 197001 (2010).
19. C. C. Homes, A. Akrap, J. S. Wen, Z. J. Xu, Z. W. Lin, Q. Li, and G. D. Gu, Phys. Rev. B **81**, 180508(R) (2010).
20. H. Luetkens, H.-H. Klauss, R. Khasanov, A. Amato, R. Klingeler, I. Hellmann, N. Leps, A. Kondrat, C. Hess, A. Köhler, G. Behr, J. Werner, and B. Büchner, Phys. Rev. Lett. **101**, 097009 (2008).
21. Chi-Cheng Lee, Wei-Guo Yin and Wei Ku, Phys. Rev. Lett. **103**, 267001 (2009).
22. Z. P. Yin, K. Haule and G. Kotliar, Nat. Mater. **10**, 932 (2011) and references therein.
23. Takuya Kato, Yoshikazu Mizuguchi, Hiroshi Nakamura, Tadashi Machida, Hideaki Sakata, and Yoshihiko Takano, Phys. Rev. B **80**, 180507 (2009).
24. T. Hanaguri, S. Niitaka, K. Kuroki, H. Takagi, Science **328**, 474 (2010).
25. A. I. Larkin and Yu. N. Ovchinnikov, Zh. Eksp. Teor. Fiz. **47** 1136 (1964).
26. P. Fulde and R. A. Ferrell, Phys. Rev. **135**, A550 (1964).
27. Y. Matsuda and H. Shimahara, J. Phys. Soc. Jpn **76**, 051005 (2007) and references therein.
28. M. A. Tanatar, T. Ishiguro, H. Tanaka, and H. Kobayashi, Phys. Rev. B **66**, 134503 (2002); S. Uji, H. Shinagawa, T. Terashima, T. Yakabe, Y. Terai, M. Tokumoto, A. Kobayashi, H. Tanaka, and H. Kobayashi, Nature **410**, 908 (2001); L. Balicas, J. S. Brooks, K. Storr, S. Uji, M. Tokumoto, H. Tanaka, H. Kobayashi, A. Kobayashi, V. Barzykin, and L. P. Gor'kov, Phys. Rev. Lett. **87**, 067002 (2001); M. Houzet, A. Buzdin, L. Bulaevskii, and M. Maley, Phys. Rev. Lett. **88**, 227001 (2002); S. Uji, T. Terashima, M. Nishimura, Y. Takahide, T. Konoike, K. Enomoto, H. Cui, H. Kobayashi, A. Kobayashi, H. Tanaka, M. Tokumoto, E. S. Choi, T. Tokumoto, D. Graf, and J. S. Brooks, Phys. Rev. Lett. **97**, 157001 (2006); K. Izawa, H. Yamaguchi, T. Sasaki, and Yuji Matsuda, Phys. Rev. Lett. **88**, 027002 (2002).
29. K. Gloos, R. Modler, H. Schimanski, C. D. Bredl, C. Geibel, F. Steglich, A. I. Buzdin, N. Sato, and T. Komatsubara, Phys. Rev. Lett. **70**, 501 (1993); G. Yin and K. Maki, Phys. Rev. B **48**, 650 (1993); M. Tachiki, S. Takahashi, P. Gegenwart, M. Weiden, M. Lang, C. Geibel, F. Steglich, R. Modler, C. Paulsen, Y. Onuki, Z. Phys. B **100**, 369 (1996); A. I. Buzdin and Kachkachi, Phys. Lett. A **225**, 341 (1997); V. F. Mitrović, M. Horvatić, C. Berthier, G. Knebel, G. Lapertot, and J. Flouquet, Phys. Rev. Lett. **97**, 117002 (2006); G. Koutroulakis, M. D. Stewart, Jr., V. F. Mitrović, M. Horvatić, C. Berthier, G. Lapertot, and J. Flouquet, Phys. Rev. Lett. **104**, 087001 (2010).
30. A. Gurevich, Phys. Rev. B **82**, 184504 (2010).
31. Y. Xia, D. Qian, L. Wray, D. Hsieh, G. F. Chen, J. L. Luo, N. L. Wang, and M. Z. Hasan, Phys. Rev. Lett. **103**, 037002 (2009).
32. V. G. Kogan, Phys. Rev. Lett. **89**, 237005 (2002).
33. M. Kidszun, S. Haindl, T. Thersleff, J. Hänisch, A. Kauffmann, K. Iida, J. Freudenberger, L. Schultz, and B. Holzapfel, Phys. Rev. Lett. **106**, 137001 (2011).
34. G. Blatter, V. B. Geshkenbein, and A. I. Larkin, Phys. Rev. Lett. **68**, 875 (1992); K. Iida *et al.*, Phys. Rev. B **81**, 100507(R) (2010).